Homogeneous and heterogeneous magnetism in (Zn,Co)O: From a random antiferromagnet to a dipolar superferromagnet by changing the growth temperature

M. Sawicki,[1,*] E. Guziewicz,[1,†] M. I. Łukasiewicz,[1] O. Proselkov,[1] I. A. Kowalik,[1] W. Lisowski,[2] P. Dluzewski,[1] A. Wittlin,[1,3] M. Jaworski,[1] A. Wolska,[1] W. Paszkowicz,[1] R. Jakiela,[1] B. S. Witkowski,[1] L. Wachnicki,[1] M. T. Klepka,[1] F. J. Luque,[4] D. Arvanitis,[5] J. W. Sobczak,[2] M. Krawczyk,[2] A. Jablonski,[2] W. Stefanowicz,[1] D. Sztenkiel,[1] M. Godlewski,[1,3] and T. Dietl[1,6,7]

[1]*Institute of Physics, Polish Academy of Sciences, al. Lotników 32/46, PL-02-668 Warszawa, Poland*

[2]*Institute of Physical Chemistry, Polish Academy of Sciences, ul. Kasprzaka 44/52, PL-01-224 Warszawa, Poland*

[3]*Cardinal Stefan Wyszyński University, Department of Mathematics and Natural Sciences College of Science, ul. Dewajtis 5, PL-01-815 Warsaw, Poland*

[4]*Depto. de Física de la Materia Condensada, Universidad Autónoma de Madrid, E-28049 Madrid, Spain*

[5]*Department of Physics and Astronomy, Uppsala University, P. O. Box 516, SE-751 20 Uppsala, Sweden*

[6]*Institute of Theoretical Physics, Faculty of Physics, University of Warsaw, PL-00-681 Warszawa, Poland*

[7]*WPI-Advanced Institute for Materials Research (WPI-AIMR), Tohoku University, 2-1-1 Katahira, Aoba-ku, Sendai 980-8577, Japan*

(Received 17 December 2012; revised manuscript received 22 May 2013; published 12 August 2013)

A series of (Zn,Co)O layers with Co contents x up to 40% grown by atomic layer deposition have been investigated. All structures deposited at 160 °C show magnetic properties specific to II-VI dilute magnetic semiconductors with localized spins $S = 3/2$ coupled by strong but short-range *antiferromagnetic* interactions resulting in low-temperature *spin-glass freezing* for $x = 0.16$ and 0.4. At higher growth temperature (200°C) metallic Co nanocrystals precipitate in two locations giving rise to two different magnetic responses: (i) a *superparamagnetic* contribution coming from volume disperse nanocrystals; (ii) a ferromagneticlike behavior brought about by nanocrystals residing at the (Zn,Co)O/substrate interface. It is shown that the dipolar coupling within the interfacial *two-dimensional* dense dispersion of nanocrystals is responsible for the ferromagneticlike behavior.

DOI: 10.1103/PhysRevB.88.085204 PACS number(s): 75.50.Pp, 68.55.Nq, 75.70.−i, 81.15.Gh

I. INTRODUCTION

Since the theoretical suggestion by *ab initio* computations that (Zn,Co)O can be intrinsically ferromagnetic,[1] and the subsequent experimental observation of high-temperature ferromagnetism,[2] this compound has reached the status of a model system for a broad class of dilute magnetic oxides (DMOs) and dilute magnetic semiconductors (DMSs).[3–6] However, over the recent years it has become more and more obvious that the understanding of these ferromagnets requires the use of advanced nanocharacterization tools in order to assess how magnetic impurities are actually incorporated and distributed depending on the growth conditions and co-doping.[7] In particular, it has become increasingly clear that in the case of a random distribution of transition metal (TM) impurities with the concentration below 10%, and in the absence of valence band holes, no ferromagnetism is expected above ∼10 K.[8–10] In fact, in many studies, including our own, of (Zn,Mn)O (Refs. 11–13) and of (Zn,Co)O (Refs. 11,14, and 15) only a paramagnetic response has been observed, affected actually by *antiferromagnetic* coupling between neighboring spins.[14–18] At the same time, it has been argued that the abundant observations of high-temperature *ferromagnetism* in DMSs and DMOs, if not originating from experimental artifacts,[19] are brought about by a highly nonrandom distribution of TM ions, introduced to the sample either purposely or *via* contamination.[7] Importantly, because of diffusion barriers, the appearance of TM-rich nanocrystals depends sensitively on the growth conditions and co-doping by shallow impurities. The nonrandom aggregation enhances dipole-dipole coupling between the nanocrystals, giving rise, specifically in two-dimensional dispersions, to ferromagneticlike response that can persist up to above room temperature.[20–22]

In the case of (Zn,Co)O, three origins of heterogeneous high-temperature ferromagnetism have been considered. First, transmission electron microscopy,[23] x-ray diffraction,[24] x-ray magnetic circular dichroism,[25] atom probe tomography,[26] and ferromagnetic resonance[27] give an evidence for the presence of metal Co inclusions. In addition, the presence of superparamagnetic behavior in Co-implanted ZnO has also been assigned to Co nanocrystals.[28] In our recent preliminary work, we found that metallic Co is located at the interface to the substrate in films showing ferromagnetic features.[29] Such interfacial metallic Co nanocrystals were recently detected by atom probe tomography[26] in (Zn,Co)O films grown by pulse layer deposition. Second, it has been suggested that the actual structure of relevant nanocrystals might be more complex, for instance, they could consist of an intermetallic ferromagnetic CoZn compound.[30] Finally, it has been argued that uncompensated spins at the surface of *antiferromagnetic* wurtzite-CoO nanocrystals could give rise to spontaneous magnetization,[31] the effect already observed in the case of NiO nanocrystals.[32] It is worth noting that according to some authors, defects or impurities rather than affecting the aggregation of Co ions, are considered to be a source of magnetic moments[20,26] or to mediate coupling between Zn-substituting Co spins.[33]

In this paper, we present results of extensive studies carried out on (Zn,Co)O samples grown by atomic layer deposition (ALD). As detailed in Secs. II–VI, as well as in

Supplemental Material,[34] the Co concentration, distribution, and aggregation have been determined by secondary-ion mass spectroscopy (SIMS); electron probe micro-analysis (EPMA); x-ray absorption near-edge structure (XANES); extended x-ray absorption fine structure (EXAFS); x-ray photoelectron spectroscopy (XPS); high-resolution transmission electron microscopy (HR-TEM) with capabilities allowing for chemical analysis, and x-ray circular magnetic dichroism (XMCD). In Sec. VII we present results of magnetic measurements carried out employing a superconducting quantum interference device (SQUID) magnetometer.

This set of experiments permits us to establish the relation between the growth parameters and the distribution of Co. Namely, when the growth process is carried out at 160 °C then the layers exhibit paramagnetic properties, that is, in a sense that the other, "legacy," II-VI DMSs did:[35–37] (i) The level structure and magnetism of single TM ions can be described (including the *c*-axis related magnetic anisotropy) by the relevant group theoretical model; (ii) their paramagnetism is weakened by strong *antiferromagnetic* superexchange among the nearest-neighbor TM cations with no evidence for ferromagnetic coupling for any pair distances, and (iii) the samples freeze to a spin-glass state on lowering temperature.

Moreover, the accumulated data indicate that interdiffusion homogenizes the Co distribution in these digital structures. In contrast, long period $(ZnO)_m(CoO)_n$ superlattices ($m = 80$, $n = 5$ or 10) show properties which can be ascribed as ZnO/(Zn,Co)O superlattices. We conclude that interdiffusion is not strong enough to randomize the Co distribution along the growth direction in the long period superlattices. Furthermore, our results demonstrate that presence of ferromagneticlike behavior is associated primarily with the growth temperature T_g. When it is risen to 200 °C or above, the ferromagneticlike response appears. It comes about in two main guises: (i) a *ferromagnetic* (FM) component which we associate with the (Zn,Co)O/substrate interface region densely populated with nanosized Co crystals and this FM is explained in terms of dipolar superferromagnetism,[22] and (ii) a relatively slowly saturating *superparamagnetic* (SP) term. We show that the relevant nanocrystals consist rather of ferromagnetic Co (or intermetallic compounds) than of uncompensated spins at the surface of antiferromagnetic CoO. Furthermore, our studies, at least so far, do not provide hints for defect- or hydrogen-mediated ferromagnetic interactions. In addition, our data for polycrystalline samples do not confirm the recently suggested[38] relation between ferromagnetism and density of grain boundaries in ZnO.

II. SAMPLES

A. Growth method

The ZnO:Co samples have been grown by ALD at substrate temperature T_g between 160 °C and 300 °C (for details see Ref. 39). The specific character of the ALD technique means that our samples are deposited as $(ZnO)_m(CoO)_n$ periodic structures with various combinations of m and n values. We grow our layers in either a digital alloy fashion ($m = 2$ or 8; $n = 1$) or employing a superlattice concept ($m = 80$ and $n = 5$ or 10). The studied films have been deposited on silicon, glass, and sapphire substrates, however, as we find no qualitative differences among them we concentrate on Si-substrate-based films.

B. Investigated samples

In Table I we display pertinent parameters characterizing growth conditions and properties of samples investigated in this study.

From XRD measurements we know that all the samples are polycrystalline layers but exhibit a homogenous wurzite-type

TABLE I. List of the samples investigated in this study. We indicate the growth temperature, the ZnO to CoO cycles' ratio, thicknesses, wurtzite *c*-axis arrangement ("random" means with no specified texture), Co concentrations obtained from SIMS, EPMA, EDX, and SQUID (when applicable), and the Hall electron concentration. This is followed by the established layers' magnetic character, when PM stands for purely paramagnetic layers (Sec. VII A), SP denotes layers where in addition to PM a sizable superparamagnetic component dominates at elevated temperatures (Sec. VII B2), and FM indicates layers which additionally show a strong and temperature-independent ferromagnetic response (Sec. VII B3). For the sake of easier identification of samples we use labeling which is given in the Alias column.

Sample	T_g (°C)	ZnO:CoO *m*:*n*	t (nm)	*c*-axis orientation	x_{Co} SIMS (%)	x_{Co} EPMA (%)	x_{Co} EDX (%)	x_{Co} SQUID (%)	Electron concentration (cm^{-3})	Magnetic behavior	Alias
F72	160	80:10	970	∥	0.8	0.74	0.8	0.7 (1.0)	3.8×10^{18}	PM	PM-S1
F73	160	80:5	1020	∥	0.6	0.62	1.2	0.7 (0.9)	3.2×10^{18}	PM	PM-S2
F53	160	8:1	560	⊥	6.6	5.4	4.8	5.0 (4.7)	2.7×10^{17}	PM	PM-1
F175	160	8:1	760	Random	5.0	5.4	5.6	6.4 (6.6)	1.4×10^{15}	PM	PM-2
F176	160	8:1	430	⊥	4.6	–	5.0	6.0 (5.9)	Highly resistive	PM	PM-3
F179	160	2:1	140	Random	15(8.9)	–	10.6	16 (14)	Highly resistive	PM	PM-4
F215	160	8:1	680	⊥	4.1	4.9	4.6	4.4 (3.8)	1.3×10^{17}	PM	PM-5
F254	160	8:1	70	Random	18-36	–	29	42 (40)	Highly resistive	PM	PM-6
F309	200	2:1	1210	Random	7	4.9	5.4	–	4.2×10^{18}	SP	SP-1
F268	200	2:1	345	Random	8	–	9.0	–	1.6×10^{16}	FM	FM-1
F307	200	2:1	250	Random	8	–	6.5	–	2.2×10^{18}	FM	FM-2
F328	200	2:1	60	Random	11.4	–	39	–	Highly resistive	FM	FM-3
F338	200	2:1	90	Random	2	–	12	–	Highly resistive	FM	FM-4

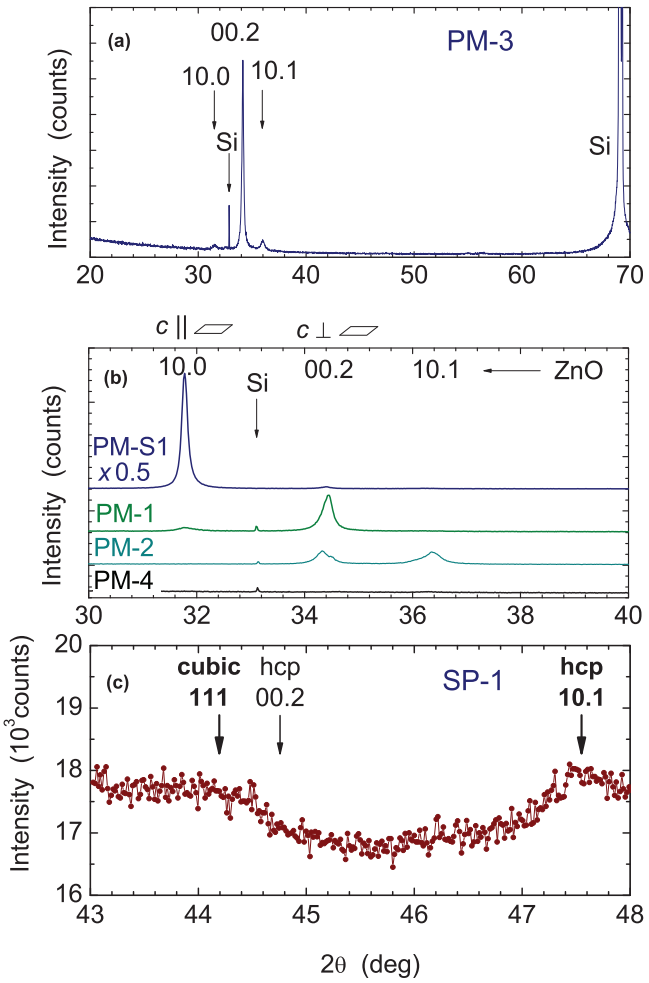

FIG. 1. (Color online) (a) XRD pattern of layer PM-3, (b) XRD pattern of four (Zn,Co)O layers: two highly textured ones (PM-1 and PM-S1) and two others without any dominant orientation of crystallites (PM-2 and PM-4). The corresponding orientation of the wurtzite c axis with respect to the sample plane are indicated at the top of the figure. (c) A result of 24-h x-ray exposure around 45° for the thickest layer ($t \simeq 1200$ nm) showing a broad and weak maxima at positions corresponding to the strongest reflexes for the cubic and hcp cobalt (marked and labeled in bolt), as well as to a weaker 10.1 reflection of the hcp structure expected at 44.76°.

(wz) structure with various textures. In the samples grown below 200 °C no traces of foreign phases are found, cobalt or cobalt oxides nanoclusters in particular, at least down to the base sensitivity of our equipment, estimated to be about 1%. Such an exemplary XRD pattern is shown in Fig. 1(a). Here, a strong 00.2 reflection indicates dominating (0001) texture, whereas weak 10.0 and 10.1 reflections show that the layer is built from 00.1 oriented crystallites; the contribution of other orientations is weak. Using the Schrerrer's formula[40] we calculate an average crystallite size which stays within 5–7 nm for most of our digital-alloy-like layers. It assumes considerably larger values of nearly 30 nm in the case of PM-S1 and PM-S2 $m = 80$ superlattices, where thick slabs of ZnO constitute a vast part of the layer. This is in line with our previous findings for ALD grown (Zn,Co)O layers[39,41] and indicates a detrimental role of Co incorporation onto the crystallographic fidelity of (Zn,Co)O.

It has already been shown that the ALD method permits one to control the texture of the ZnO films.[12,39,41] As displayed in Table I and shown in Fig. 1(b), textured films with dominant orientation of the c axis along the growth direction (e.g., PM-1 and PM-3), perpendicular to it (e.g., PM-S1), or films with no texture (samples PM-2 and PM-4) can be prepared. As the c-axis orientation determines the type of magnetic anisotropy exerted by the layers we investigate this issue in greater detail in Sec. VII A4 showing, in particular, that it is possible to extract quantitative information on the c-axis distribution using low-temperature magnetometry.

In the course of our studies we find that it is the growth temperature of 200 °C and above that plays the decisive role in the development of nonparamagnetic features in our layers. In general, the detection of nanocrystalline magnetic precipitates in semiconductors by modern laboratory diffractometers is daunting.[42] Nevertheless, broad and weak x-ray signatures of metallic Co at $2\theta \approx 44.5°$ were resolved for (Zn,Co)O grown at 450 °C, in which a mean Co nanocrystal size was presumably as large as 8 nm.[24] We have been unable to detect such signatures in our films grown at 200 °C, where nanocrystals are smaller, except for the thickest film ($t = 1210$ nm), as shown in Fig. 1(c). Despite a 24-h exposure the Co signal only marginally exceeds the noise level. From a rough estimate of the peak width (at least 1°) we get the contributing nanocrystal diameter of about 8 nm, much larger than that established from magnetic studies, 2.5 nm in this superparamagnetic sample, meaning that most likely we are able to detect only the largest nanocrystals from the tail of their size distribution. A similar scan around 77° and wider scans for other layers give featureless flat responses.

III. XANES AND EXAFS INVESTIGATIONS

We have performed comparative studies at the K edge of Co for the PM-6 (paramagnetic) and FM-3 (ferromagnetic) (Zn,Co)O samples. The description of the experimental results is performed employing the IFEFFIT data analysis package making use of the ATHENA and ARTEMIS codes.[43] Since the hard x rays in question penetrate the whole film, Co atoms in all spatial locations contribute to the signal. As shown in Fig. 2, we compare the measured XANES spectra with the results of *ab initio* computations carried out for (Zn,Co)O employing the FEFF9.5 code[44,45] as well as with the spectrum for metallic Co. These data imply that in both samples the majority of Co atoms occupy Zn-substitutional positions. At the same time, however, differences in spectra between the paramagnetic and ferromagnetic samples point to the presence of a certain amount of metallic Co in the case of the ferromagnetic film.[39,46] In particular, the contribution of metallic Co is seen as a weakening of the pre-edge peak, as also observed for (Zn,Co)O grown by other methods.[23]

In Fig. 3, the Fourier transforms of the EXAFS spectra and their fits are collected for the two studied samples. The fitting is performed in the R range from 1 to 3.5 Å. In the case of paramagnetic sample PM-6, the first two maxima are well described by coordination spheres expected for ZnO, i.e., four

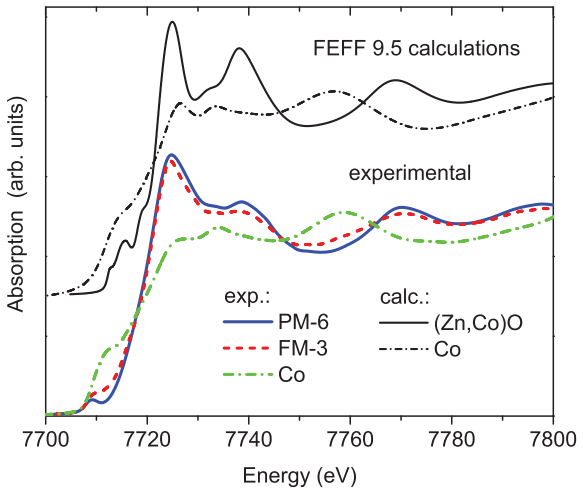

FIG. 2. (Color online) Experimental and computed XANES spectra of the investigated samples. Spectra of the metallic Co (calculated and measured) are shown for comparison. Experimental and simulated spectra are shifted vertically for clarity.

oxygen atoms at the distance of 1.97(2) Å and six zinc atoms at the distances of 3.19(1) Å and 3.23(1) Å, respectively. In the ferromagnetic FM-3 layer a new peak appears between the two maxima corresponding to the ZnO lattice which is a clear indication for the presence of another crystallographic phase-metallic Co in this case. It has been found from the fitting that about 73% of Co atoms form (Zn,Co)O and 27% contribute to metallic Co in this sample.

To conclude, XANES and EXAFS experiments show a different Co local structure for paramagnetic and ferromagnetic (Zn,Co)O samples. In paramagnetic films Co ions occupy substitutional Zn positions, whereas in ferromagnetic ones, only a part of Co ions substitute zinc whereas the rest is in a metallic form. To establish where metallic Co is located in the layer we have employed XPS profiling, discussed in the next section.

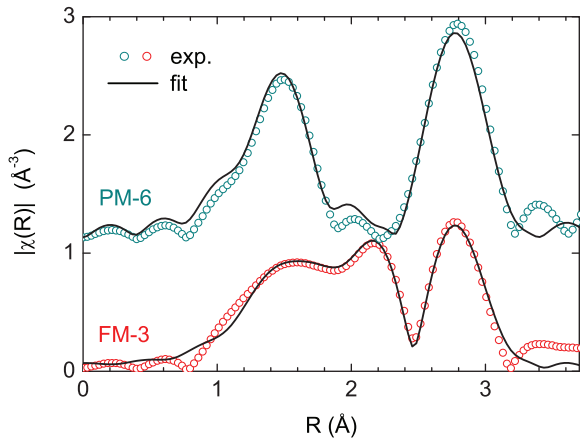

FIG. 3. (Color online) Magnitude of the Fourier transform of the EXAFS spectra and fitting results for the samples. Spectra are shifted vertically for clarity.

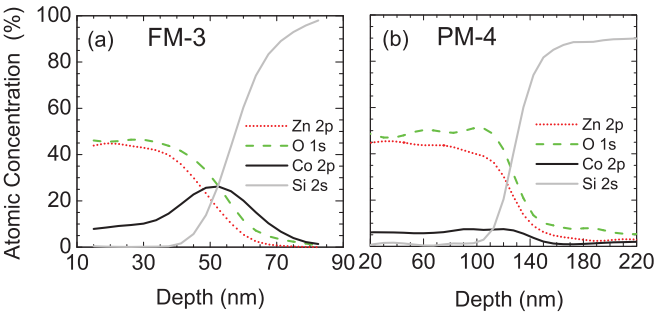

FIG. 4. (Color online) XPS sputter depth profiles of the (a) ferromagnetic and (b) paramagnetic (Zn,Co)O films.

IV. XPS INVESTIGATIONS

We have performed the XPS studies in order to determine the chemical state of cobalt in (Zn,Co)O films and to establish the location of Co within the layer. XPS is a surface sensitive technique in which the probing depth depends on the kinetic energy of photoelectrons, but in any case does not exceed a few nanometers.[47] Therefore we perform elemental depth profiles that are presented in Figs. 4(a) and 4(b) for FM and PM films, respectively. All profiles reveal the elemental distribution in bulk of films from 15-nm depth until the (Zn,Co)O/Si interface was reached. The relative atomic concentration of zinc, oxygen, cobalt, and silicon are evaluated from the intensity of XPS peaks associated with the Zn2p, O1s, Co2p, and Si2s core levels. Cobalt distribution is found to be different for PM and FM samples. In the ferromagnetic (Zn,Co)O films a substantial enhancement of the Co concentration is found in the (Zn,Co)O/Si interface region, as shown in Fig. 4(a). The cobalt concentration there is estimated to be more than three times larger than in the rest of the film. Such a Co-rich interfacial layer is not observed in the paramagnetic (Zn,Co)O films [Fig. 4(b)].

In order to elucidate the chemical nature of cobalt containing phases formed in the (Zn,Co)O films we analyzed the high-resolution XPS spectra of the Co2p, which have been taken at sequential steps of depth-profiling processing: at the surface of the (Zn,Co)O film, after removing the 15 nm of the (Zn,Co)O layer from the top and at the (Zn,Co)O/Si interface. The last two results are presented in Fig. 5. The original $Co2p_{3/2}$ spectra are presented together with deconvoluted peaks. Three forms of cobalt compounds can be distinguished in both samples at a depth of 15 nm (Fig. 5, bottom). The strongest component, situated at BE = 780.3 eV, is characteristic for cobalt oxide.[48] Two forms of cobalt oxides are stable in air at room temperature: CoO and Co_3O_4.[48,49] The Co2p spectra recorded during Ar^+ depth profiling of both samples show strong satellites what indicate CoO to be a main cobalt oxide component. This means that the Co atoms that substitute Zn in the ZnO matrix, ZnO:Co, contribute to this component. Another $Co2p_{3/2}$ XPS state is located at BE = 781.8 eV. Its chemical shift is characteristic of cobalt surrounded by −OH groups.[48,49] The $Co2p_{3/2}$ contribution at the BE = 777.8 eV can be assigned to metallic cobalt.[48] This observation indicates that some Co atoms in the (Zn,Co)O layers form metallic clusters and that these clusters are present in both ferromagnetic and paramagnetic films. However, based on magnetic

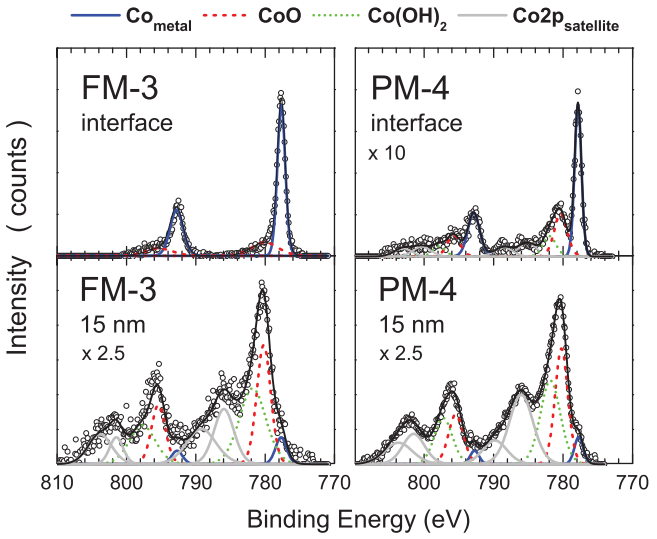

FIG. 5. (Color online) Co2p core level XPS spectra measured during Ar^+ sputter profiling after removing of 15 nm of the (Zn,Co)O film (bottom) and at the (Zn,Co)O/Si interface region (top). (Left) Ferromagnetic (sample FM-3); (right) paramagnetic (sample PM-4) (Zn,Co)O film. Deconvoluted spectra indicate different chemical states of Co compounds.

data (Sec. VII A), it appears that in samples deposited at low temperatures the total number and/or the size of metallic Co inclusions is too small to produce a detectable response, even on the background of a weak paramagnetic signal.

A significant difference between paramagnetic and ferromagnetic films is observed in the region of the (Zn,Co)O/Si interface (see Fig. 5, top). In the FM film we observe mainly metallic cobalt accompanied by a very small concentration of CoO in the interface region. The absence of shake-up satellites, which is a characteristic feature of XPS spectra of metallic transition metals and rare earth, indicates the metallic Co to be a dominant chemical state, what means that the cobalt oxide contribution is very small. In the PM (Zn,Co)O film, a metallic contribution is accompanied by cobalt oxides and Co-OH bonds, but also in this case the contribution from metallic cobalt is larger than in the volume of the sample.

In conclusion, the analysis of XPS spectra showed that inclusions of metallic cobalt clusters have been detected in both paramagnetic and ferromagnetic (Zn,Co)O samples. A different Co-cluster distribution has been observed within the (Zn,Co)O/Si interface region of both films. The interface in the ferromagnetic (Zn,Co)O film is formed mainly by accumulated metallic Co, whereas in the paramagnetic films the metallic Co is accompanied by cobalt oxides and hydroxides.

V. HR-TEM INVESTIGATIONS

Since both SIMS (see Supplemental Material) and XPS studies point to a presence of Co-enriched regions of our layers we perform detailed high-resolution transmission electron microscopy (HR-TEM) studies. Only digital alloy $(ZnO)_m$/CoO layers have been investigated by TEM. All the samples reveal a 2- to 3-nm thick amorphous SiO_2 layer covering the Si(001) substrate, on which the (Zn,Co)O films are grown.

The HR-TEM microstructural analysis permits us to classify our layers into two main categories. The first one, characteristic for layers grown at 160 °C, exemplified in Fig. 6(a) for layer PM-4, exhibits a uniform structure with oval, 5–10 nm in size, monocrystalline grains. These values compare very well with the average grain size established from XRD. All these grains show a wurtzite structure characteristic of ZnO films, as can be seen in the inset of Fig. 6(a). This homogenous polycrystalline structure is observed at first 40–50 nm from the layer/Si interface. In the next part of the film the columnar growth takes place and the width of the columns ranges from 25 to 30 nm. No Co-rich volumes are found.

The second category, characteristic for layers grown above 160 °C, exhibits smaller oval crystallites (diameter of 3–4 nm) at the first 40–50 nm of the layer and narrower nanocolumns (10–22 nm in width) in the rest of the layer. However, the basic difference between these two types of samples lies in the existence of a layer of Co clusters, 3–4 nm in diameter, located at the layer/substrate interface, as exemplified in Fig. 6(b) for layer FM-3. The closeup on one such cluster presented in the inset to Fig. 6(b) reveals the fcc crystallographic structure characteristic of metallic cobalt. So, the HR-TEM characterization fully confirms the conclusion derived from XPS studies about a large quantity of metallic cobalt present at the interfacial region of such films. It is shown later (Sec. VII B3) that just this layer of Co clusters is responsible for a robust, nearly temperature-independent and highly anisotropic ferromagnetic response. The point chemical analysis of another layer of this type presented in Supplemental Material gives evidence of the existence of Co-rich volumes also in the bulk of the layer.

VI. XAS AND XMCD INVESTIGATIONS

We now describe results of x-ray absorption spectroscopy (XAS) and XMCD measurements at the I1011 beamline of the MAX-lab synchrotron radiation laboratory,[50] focusing on the Co L edge and O K edge. We investigate at room temperature the same ferromagnetic sample FM-3 as in the XPS studies, which contains a crater etched down to the layer/substrate interface (see Sec. IV). Owing to a limiting penetration depth of the soft x rays in question, by probing separately the free surface of the layer and the layer/substrate interface (locations A and B, respectively, as marked in Fig. 7) we have access to disentangled element-specific information in these two regions.

In the case of XAS studies, linearly polarized x rays are used yielding a higher photon flux. We do not find any traces of Ti, V, Mn, Cr, Fe atoms in the sample. The content of Co in the "bulk" part of the layer is 6% on average, calculated by using the tabulated atomic cross sections for XAS. The distribution of Co is not homogeneous within the layer. The highest amount of Co is about 14%, which is close to the value obtained from the analysis of the XANES data.

As presented in Fig. 7, we find sizable differences in the fine structure of the Co white lines for the surface and the interface regions. The Co L edge obtained at the surface region and around the rim of the crater shows a typical multiplet shape, reported previously for (Zn,Co)O.[51] Another chemical composition and electronic structure is observed within the

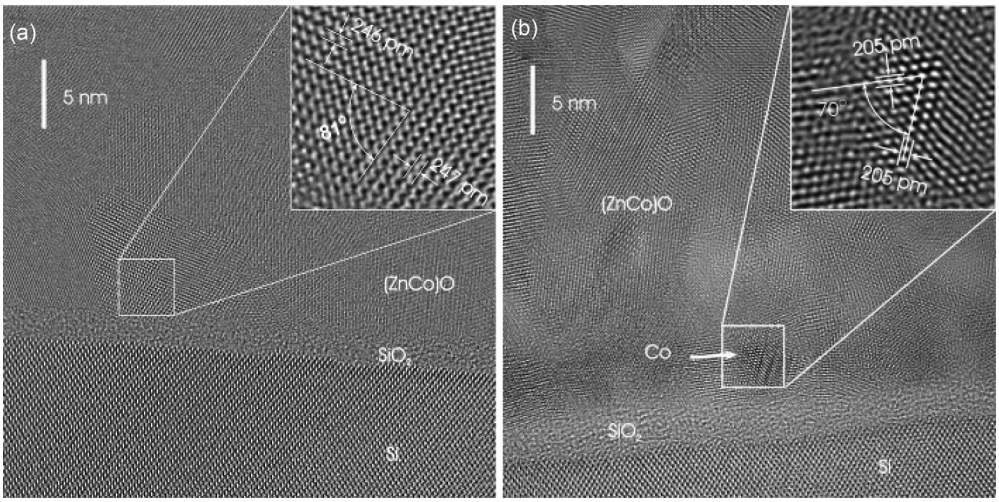

FIG. 6. High-resolution transmission electron microscopy images of (a) PM-4 sample with (Zn,Co)O wurtzite particle projected in the ⟨01.1⟩ direction, and (b) FM-3 sample with Co fcc nanocrystal projected in the ⟨011⟩ direction.

crater. In particular, the interpeak continuum of final states (of *s* symmetry) for the Co spectra is stronger in the crater. Since the magnitude of final state continuum is a direct probe of the degree of metallic character, we conclude that Co may form either a continuous ultrathin film or a layer of nanocrystals at the interface. At the same time, the shape of XAS spectra indicates that in the interface region the metallic Co is the dominant phase but not the only one, as we detect also a contribution specific to CoO.[52] More quantitatively, the area under the Co L_3 line (Fig. 7) corresponding to the surface and interface region is, respectively, 2.5 and 1.25 times larger than expected for metallic Co. This shows that while Co is mostly metallic at the interface, still about 17% of Co atoms is in a $2+$ state. At the same time, a certain amount of Zn has also been found at the interface, showing that metallic Co coexists with (Zn,Co)O.

As shown in Fig. 8, an XMCD dichroic signal is seen in the interface region, when the magnetic field of 350 Oe is applied along the film plane. The presence of XMCD in such a small magnetizing field indicates that interfacial Co may account for ferromagneticlike response at 300 K in (Zn,Co)O grown at high temperatures.

A metallic state from the Co L-edge XAS and XMCD features was also observed earlier for ZnCoO thin films prepared by pulsed laser deposition at 400°C and 500°C.[53] For

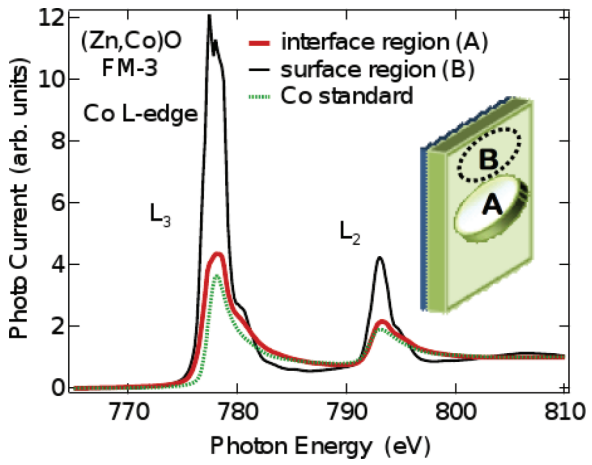

FIG. 7. (Color online) L-edge x-ray absorption spectra versus photon energy for (Zn,Co)O from the interface region (region A, in the crater) and from the surface region (region B of the film); the Co L-edge data are taken at normal x-ray incidence (a 90° angle between the x-ray propagation direction and the film surface plane) in the total electron yield mode and normalized to the atomic continuum at high photon energies.

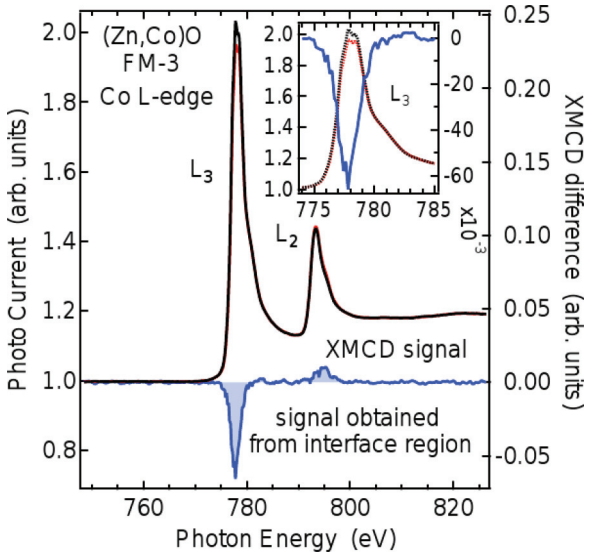

FIG. 8. (Color online) XAS (left scale) and XMCD (right scale) spectra in the total electron yield mode versus photon energy. Measurements are performed at room temperature under an applied magnetic field of $H = 350$ Oe. The XAS spectra are obtained with nearly fully circularly polarized light (a light helicity of 0.85); a 40° x-ray incidence angle is employed. The insert shows an enlarged view of the L_3 edge of the XAS and XMCD spectra.

these spectra, bulk sensitive fluorescence yield was used in the soft x-ray regime. In agreement with our own conclusions the metallic state for the Co atoms deep in the thin film bulk, was explained by the presence of metallic Co precipitates.[53]

VII. SQUID INVESTIGATIONS

Having determined the Co distribution in our (Zn,Co)O layers we turn to investigations of macroscopic magnetic properties. According to the data presented below, magnetization $M(T,H)$ of samples grown at 160 °C shows a paramagnetic (PM) behavior, which can be entirely described assuming that Co ions occupy only Zn-substitutional positions and that the spin-spin interaction is an antiferromagnetic short-range superexchange, as in canonical II-VI Co-based DMSs. On the other hand, in samples grown at higher temperatures, at which the nanocharacterization reveals metallic Co aggregation, two additional contributions to $M(H)$ can also be observed: (i) a fast saturating, highly anisotropic, and temperature-independent *ferromagnetic* (FM) component and (ii) a relatively slowly saturating *superparamagnetic* (SP) term.

A. Magnetization of Zn-substitutional Co ions

1. Theoretical modeling

Properties of a single Zn-substitutional Co^{2+} ion (d^7) in wurtzite-ZnO can be described by the general $S = 3/2$ Hamiltonian.[54] Details of the modeling are given in Supplemental Material.

Here, we consider the temperature dependence of magnetic susceptibility. The presence of spin-spin interactions can be taken into account within the high-temperature expansion.[55] This procedure leads to the Curie-Weiss law which, for a random distribution of localized spins, is parametrized by two constants, C_0 and Θ_0 independent of the Co concentration x,

$$\chi(T) = xC_0/(T - x\Theta_0), \tag{1}$$

where

$$\Theta_0 = -\frac{1}{3}S(S+1)\sum_j z_j J_j. \tag{2}$$

Here, the summation extends over the subsequent cation coordination spheres; z_j is the number of cations in the sphere j, and $J_j \equiv J_{ij}$ is the corresponding Co-Co exchange integral in the Hamiltonian $H_{ij} = -J_{ij}\boldsymbol{S}_i\boldsymbol{S}_j$. We note that in another convention twice smaller values of J_j are considered and then the factor 1/3 in Eq. (2) is replaced by 2/3. Furthermore, an effective nearest-neighbor exchange energy J_{eff} is sometimes introduced in the literature, in terms of which

$$\Theta_0 = -\tfrac{1}{3}S(S+1)z_1 J_{\text{eff}}. \tag{3}$$

The values of the Landé factors quoted above point to an average value of the Landé factor $\langle g\rangle = 2.25$, suitable to describe polycrystalline samples. For this magnitude of $\langle g\rangle$ we obtain the Curie constant $C = xC_0$, where $C_0 = 0.17$ emu K/cm^3.

The high-temperature expansion is valid as long as $T \gg |\Theta|$, where the Curie-Weiss temperature $\Theta = x\Theta_0$. In a wider temperature range, $\chi(T)$ of random antiferromagnets is well described by[56,57] $\chi(T) = aT^{-\alpha}$, where a is a temperature-independent constant and $\alpha < 1$.

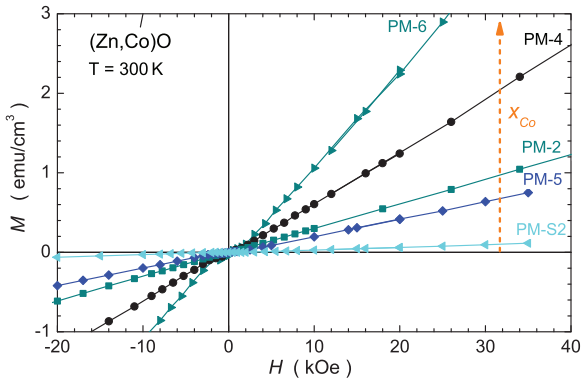

FIG. 9. (Color online) Room temperature $M(H)$ for selected paramagnetic (Zn,Co)O layers. All data show a good linearity in H, except the low field region where a (negative) residual sigmoidal signal mars the otherwise paramagnetic $M(H)$. This spurious nonlinearity near $H = 0$ results from a spread of magnitudes of the nonlinear components to m exhibited by the Si substrates we use (see Fig. 1 in Supplemental Material). The arrow indicates the direction of the growth of the Co content in these layers.

2. Temperature dependence of magnetic susceptibility

Figure 9 presents room temperature dependence of (volume) magnetization $M(H)$ on the applied field H for selected (Zn,Co)O layers grown at 160 °C, where M is obtained from m using the whole thickness of the deposited structure to assess the volume of the investigated layer. The main message of this graph is that all these layers show, at strong fields, a linear $M(H)$, a dependency expected for an atomic-spin paramagnet at elevated temperatures, and so that ferromagnetic or superparamagnetic contributions are negligibly small in these films. Samples exhibiting such properties are denoted as "PM" in Table I. We note that if a sample exhibits such a linear $M(H)$ at room temperature, then *no* traces of ferromagnetic components are seen down to the base temperature of the magnetometer, $T \approx 2$ K. In other words, if a ferromagnetic response is present, it persists to above room temperature independently of a nominal Co concentration. Finally, our data push the bar for the absolute value of the Co solubility limit in ZnO to above 40%, simultaneously indicating that the much lower values quoted in the literature (even below 10%) correspond to higher growth temperature than those employed in the present study.

We start our quantitative analysis from magnetic susceptibility $\chi(T)$, whose temperature dependence is obtained from $M(H,T)$ data measured below 10 kOe. The values of $\chi(T)$ determined in this way are plotted in a double logarithmic scale in Fig. 10. The data indicate that $\chi(T) \propto T^{-\alpha}$, where $\alpha < 1$, and its magnitude decreases with x, as shown in the inset. Such a dependence is characteristic for random antiferromagnets, that is, for paramagnetic compounds with a wide spectrum of (antiferromagnetic) exchange integrals.[56,57] The upper bound of this spectrum, i.e., an effective nearest-neighbor exchange integral J_{eff}, can be evaluated by analyzing χ^{-1} vs T in terms of the high-temperature expansion [Eq. (1)].

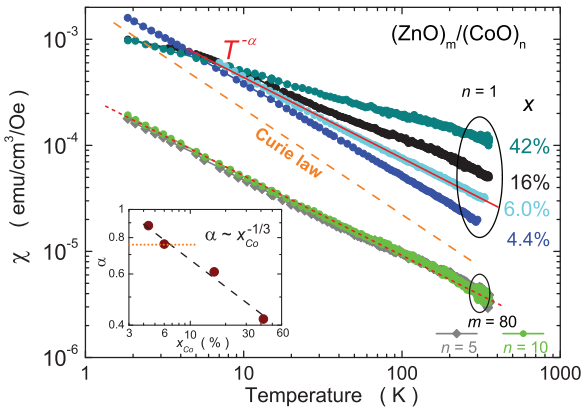

FIG. 10. (Color online) Temperature dependence of magnetic susceptibility. The data sets are labeled by the Co concentration x, established for digital alloy layers and by their periods for two superlattices. The dashed line indicates the Curie law $\chi(T) \propto 1/T$. Solid and dotted lines indicate that $\chi(T) \propto T^{-\alpha}$, where $\alpha < 1$, the dependence specific for a random antiferromagnet. The values of α established in this way for the upper bunch of curves are plotted vs x in the inset. The dashed black line shows $\alpha \propto x^{-1/3}$, and serves as a guide for the eye. This trend is not obeyed for the samples grown in a superlattice fashion, for which the magnitude of χ is low ($x \approx 0.7\%$), whereas α (marked as dotted line in the inset) corresponds to $x \approx 6\%$.

As shown in Fig. 11, the inverse of $\chi(T)$ points to a negative sign of the Curie-Weiss temperature Θ, which reconfirms the antiferromagnetic character of spin-spin interactions. Slopes of $1/\chi(T)$ vs T dependencies provide the values of Co concentrations x listed in Table I. Furthermore, according to Eqs. (1) and (2), the extrapolated values $\chi^{-1}(T = 0)$ for randomly distributed spins should be independent of x and directly proportional to the exchange integrals characterizing the spin-spin coupling. And the data gathered in the main part of Fig. 11 instruct us that this is the case for the layers grown in the digital alloy fashion, indicating that independently of the Co content such a growth mode leads to films with randomly distributed Co cations over the ZnO host lattice.

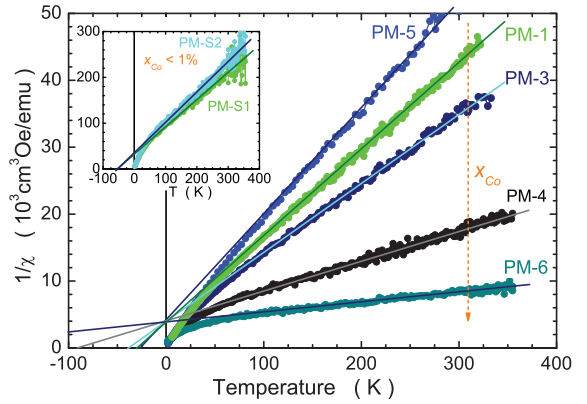

FIG. 11. (Color online) The inverse of the magnetic susceptibility χ as a function of temperature for paramagnetic (Zn,Co)O layers. The main panel groups data for layers in which CoO layers were introduced in a digital way, whereas the inset presents data for the two layers grown in a superlatticelike fashion. Note the substantially different values of $\chi^{-1}(T = 0)$ for the two types of samples.

3. *Long period $(ZnO)_m(CoO)_n$ superlattices*

It appears to be an altogether different story with the long period $m = 80$, $n = 5$ and 10 superlattices. As evidenced in Figs. 10 and 11 their $\chi(T)$ stick out completely from those of the layers grown in the digital alloy manner. In fact, a simple simulation for PM-S1 sample shows that the absolute values of $\chi(T)$ can be well reproduced assuming 8:1 partition ratio between pure ZnO and $Zn_{1-x}Co_xO$ sublayers with x = 6% in a rectangular ZnO/$Zn_{1-x}Co_xO$ superlattice, indicating that interdifussion is not strong enough to homogenize the Co content along the growth direction in such long period superlattices.

4. *Magnetic anisotropy*

Electron paramagnetic resonance (EPR),[54] optical absorption,[58] and direct magnetometry[15,16] prove the existence of a sizable low-temperature magnetic anisotropy in $Zn_{1-x}Co_xO$. Here we examine samples for which XRD measurements [Fig. 1(b) in Sec. II B] have revealed the wealth of various c-axis arrangements. The experimental data shown in Fig. 12 (symbols) for parallel and perpendicular directions of the magnetic field with respect to the film plane demonstrate that magnetization anisotropy follows the trend expected theoretically (lines) for the distribution of c axis revealed by the XRD measurements. In particular, in the textured films the magnitude of magnetization is larger for the magnetic field perpendicular to the prevailing direction of the c axis [Figs. 12(a) and 12(b)]. The description of these data has been carried out following the model presented in Sec. II A of Supplemental Material, where the parameter y quantifying the fraction of the crystal grains having their c axis along the growth direction has been introduced. According to the fitting procedure, it attains the value of 0.54 in sample PM-1, for which XRD reveals that the c axis is mostly out of the film plane, whereas $y = 0.10$ in the case of sample PM-S1, where the c axis is preferably oriented in-plane of the film. In contrast, magnetization is isotropic [Figs. 12(c) and 12(d)] in the case of samples that are polycrystalline according to the XRD results.

Finally, we want to emphasize a value of the analysis presented here of the low-temperature $M(H)$ as an accurate method for determining the degree of the crystallographic order in polycrystals exhibiting a strong magnetocrystalline anisotropy. However, one has to keep in mind that experimental handling of very thin layers is tricky in any circumstances, and despite a quite strong magnetic anisotropy in (Zn,Co)O, a "slight" error in the substrate contribution can markedly change the input data for fitting and so invalidate the magnetic assessment of the c-axis ordering.

5. *Quantifying spin-spin interactions*

It is well known that extrapolation of $\chi^{-1}(T)$ to zero provides magnitudes of Curie-Weiss temperatures for particular samples. Now, assuming that the Co-Co coupling can be characterized by a single exchange energy describing the interaction with 12 nearest neighbors, for the experimental value of $\chi^{-1}(T = 0) = -\Theta_0/C_0 = 4200 \pm 400\,\mathrm{cm}^3/\mathrm{emu}$ we obtain $\Theta_0 = -700 \pm 70$ K and $J_{\mathrm{eff}} = 47 \pm 5$ K. This value compares favorably with 42, 51, and 53 K obtained for single crystalline thin films[16] (when we restore the omitted factor

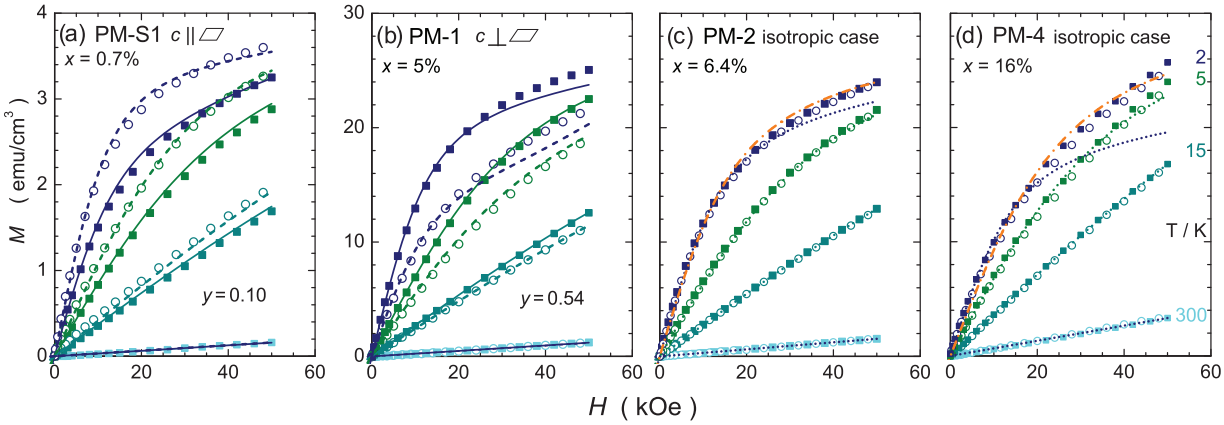

FIG. 12. (Color online) Magnetization for a series of samples measured at 2, 5, 15, and 300 K [from top to bottom, indicated in panel (d)] for two orientations of the magnetic field: in-plane (solid squares) and perpendicular to the sample plane (open circles). Lines show modeling of the data by theory outlined in Sec. VII A1. The solid and dashed lines in panels (a) and (b) are calculated for the mixed anisotropy case considering the in-plane and perpendicular magnetic field, respectively. The fraction y of grains with the c axis perpendicular to the film plane and the effective Co concentration $x_{\mathrm{eff}}(T)$ are the fitting parameters, whose values are displayed in panels (a) and (b) and in Table II, respectively. The dotted lines in panels (c) and (d) represent the isotropic (randomized with respect to the c axis) values of magnetization in polycrystalline films. The orange dashed-dotted lines represent a considerably improved fit with an effective temperature T_{AF} added to the calculations performed at the lowest temperature and displayed in Table II.

"2" in their definition of J_{nn}), single phase bulk crystals[11] and powders[59] (after a necessary adjustment of the material parameters to the values adopted in this study), respectively.

Interestingly, all these values are nearly 40% smaller than that established for bulk wz-(Cd,Co)S (Ref. 36) and twice smaller than those found in bulk zinc-blende (Zn,Co)S and (Zn,Co)Se (Ref. 60). This implies another dependence of $|\Theta_0|$ on the bond length d comparing to the case of Mn-based II-VI DMS, where Θ_0 tends to decrease monotonically with d.[11,55]

The quantitative description of $\boldsymbol{M}(\boldsymbol{H},T)$ provides also the values of x_{eff} and T_{AF}, collected in Table II. These parameters supply also information on spin-spin coupling.[61,62] In particular, the magnitudes of x_{eff} determined at 2 K are in agreement with the concentrations of Co ions having no other Co as the nearest neighbor (see Sec. VII A1). This means that there is a strong antiferromagnetic coupling between Co ions occupying any of the 12 nearest-neighbor positions in the cation sublattice. At the same time, much lower values of T_{AF}(2 K), comparing to high-temperature Curie-Weiss Θ, indicate that coupling to next nearest neighbors is relatively weak, which points to a rather short-range character of the antiferromagnetic spin-spin interactions.

Altogether, the findings accumulated so far support the results of those *ab initio* simulations which do *not* predict the presence of ferromagnetic interactions at any distance of Co-Co pairs.[63,64]

TABLE II. Temperature dependence of the effective Co concentration x_{eff}, given here as a ratio to its value x at 300 K, for the four samples presented in Fig. 12. This is followed by a line giving the statistically expected fraction of single Co cations present in the wurtzite lattice at given x, corrected in the case of the superlattice sample (PM-S1) by the period ratio (Sec. VII A3). The bottom line lists the values of effective temperatures T_{AF} added to the calculations of $\boldsymbol{M}(\boldsymbol{H},T)$ for two samples with the highest x (PM-2 and PM-4) at 2 K.

T(K)	PM-S1 –	PM-1 5.0%	PM-2 6.4%	PM-4 16%
300	1.00	1.00	1.00	1.00
15	0.51	0.61	0.45	0.27
5	0.50	0.53	0.38	0.19
2	0.49	0.51	0.35	0.14
$2 + T_{\mathrm{AF}}$	–	–	0.37	0.18
Singles	0.92	0.54	0.45	0.14
T_{AF}(2 K)	–	–	0.35 K	1.45 K

6. *Spin-glass freezing*

Since the very early stage of magnetic studies of DMSs, low-temperature cusps on $\chi(T)$ curves were observed over a broad range of magnetic cation concentration.[65–67] Despite the lack of competing interactions, but on account of the presence of positional disorder and spin frustration, these materials exhibit spin-glass characteristics driven entirely by antiferromagnetic interactions.[68] And our two paramagnetic layers with the highest Co content show a weak low-temperature feature that closely resembles previous findings in other DMS compounds.[65–67] Figure 13 collects zero-field cooled magnetization (ZFCM), field-cooled magnetization (FCM), and thermoremnant magnetization (TRM) for these layers. A typical transition to a glassy state bifurcation on ZFCM and FCM is seen. However, a strong paramagnetic background masks the effect of freezing (characteristic cusp on the ZFCM) considerably, therefore the TRM measurement serves to accurately establish the freezing temperature T_{f} for these layers.

An important question arises now whether the history-dependent effects presented here and a very weak magnetic hysteresis developing at $T < T_{\mathrm{f}}$ (not shown) are indeed related to the spin-glass-like freezing, or are a manifestation of the dynamical blocking of some small ferromagnetic clusters (Co-metal droplets or some Co-rich spinel precipitates) that

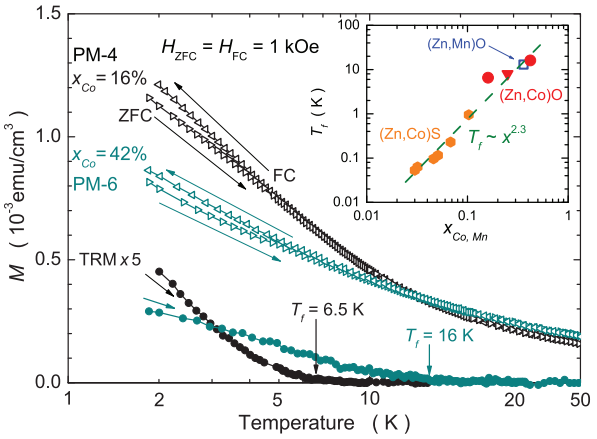

FIG. 13. (Color online) (Main figure) A spin-glass-like behavior of two paramagnetic layers with the highest Co content. (Darker color) PM-4, $x \cong 16\%$; lighter one, PM-6, $x \cong 42\%$. Zero field cooled magnetization (ZFCM) and field cooled magnetization (FCM) measurements performed at 1 kOe, are indicated by arrows and marked by open triangles pointing towards increasing or decreasing temperature, respectively. Solid circles mark thermoremanent magnetization (TRM) (magnified 5 times for better presentation). Inset shows T_f dependence on the transition metal content: x_{Mn} in (Zn,Mn)O, open square from Ref. 69; x_{Co} in (Zn,Co)S, solid hexagons from Ref. 70; and in (Zn,Co)O, solid triangle from Ref. 14 and bullets from this study.

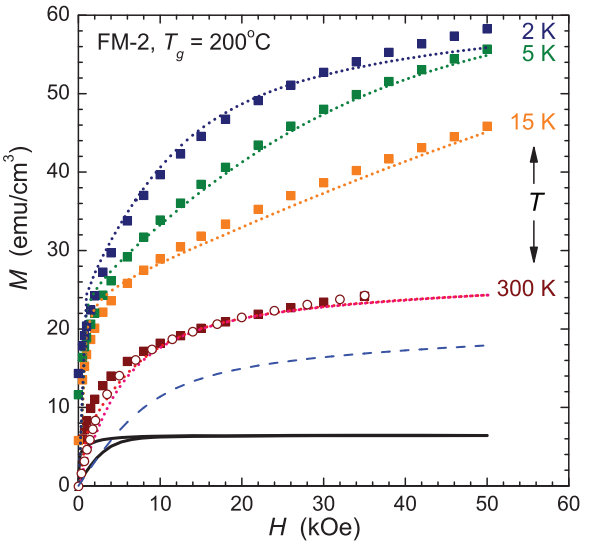

FIG. 14. (Color online) A representative (volume) magnetization for a layer grown at 200 °C (FM-2) measured at 2, 5, 15, and 300 K. Solid squares are obtained with the magnetic field applied parallel to the sample plane. For clarity the data obtained in perpendicular configuration are shown only for 300 K (open circles). Dotted lines indicate results of the modeling which assumes a presence of three independent magnetic contributions: PM, SP, and FM (planar superspin glass) one, as detailed in the text. The dashed line represents the magnitude and room temperature curvature of the superparamagnetic component, whereas the two solid lines represent (derived from sample FM-3) the ferromagneticlike component (with its anisotropy) (see Sec. VII B3).

together give rise to superparamagneticlike behavior. In order to resolve this issue one should resort to studies of the long-time-scale dynamics of the nonreversible part of the signal,[71] but the presence of a large PM background renders such an experiment problematic. However, we argue for the spin-glass freezing on the account of the minute magnitude of M, corresponding solely to the PM response of these two samples. We note that if sizable and numerous Co-rich metallic (ferromagnetic) inclusions were present they would dominate the magnetic response at weak magnetic fields (at any temperature) considerably increasing the magnitude of M, see, e.g., Ref. 72 (for broader discussion see Supplemental Material).

Finally, we find a good correspondence between the freezing temperatures observed here with those reported for similar systems. As indicated in the inset to Fig. 13 established here T_{f} values follow the already established exponential dependency $T_f \sim x^{\alpha}$ with $\alpha = 2.3 \pm 0.4$ for bulk (II,Co)VI compounds.[70] Recently, the same $\alpha = 2.2$ was found to govern the Curie temperature dependency on x_{Mn} in (Ga,Mn)N.[10] This correspondence highlights the fact that both compounds belong to dilute magnetic insulators,[73] in which the absence of electrons and holes makes carrier mediated spin-spin coupling irrelevant,[74] and the lack of mixed valence—all magnetic ions are in the same 3+ charge state—precludes the presence of double exchange.[75,76] Therefore, the same superexchange accounts for spin-spin interactions.[77–79] The scaling exponent α is then found from relation[80] $\alpha = \lambda/D = 2.3 \pm 0.2$, since the exponent governing the spatial dependence of the interaction $\lambda = 6.3 - 6.8$ in Co- and Mn-containing DMS,[67,70] and $D = 3$ is the dimensionality.

B. Magnetism in heterogenous (Zn,Co)O

1. *Experimental*

We turn now to layers grown at higher temperatures ($T_{\mathrm{g}} \geqslant 200\,^{\circ}\mathrm{C}$). Points in Fig. 14 represent experimental $M(H,T)$ gathered at wide field and temperature range for layer FM-2, a representative example of these layers which host the nanocrystals both in its volume and at the interface with the substrate. We can phenomenologically reproduce the whole experimental data set by a straight sum of three contributions: paramagnetic, superparamagnetic, and ferromagnetic (for broader discussion see Supplemental Material). The results of the modeling are marked in Fig. 14 by dotted lines and are calculated as follows.

The PM contribution, originating from substitutional Co ions, is calculated according to the method described in the previous section. In particular, due to a nearly isotopic low-temperature $M(H)$ we use the isotropic paramagnetic $M(T,H)$, allow for the temperature dependence of x_{eff}, and take $T_{\mathrm{AF}} = 0$ for simplicity. The magnitude of the PM signal is parametrized by the concentration of Co cations, x_{eff}(300 K).

The SP contribution to $M(T,H)$ is approximated by the Langevin function $N_{\mathrm{SP}}\mu L(x)$, where $x = \mu H/k_{\mathrm{B}}T$ and N_{SP} is the density of monodisperse nanocrystals hosting the superspins of magnitude $\mu = NS$, where N is the number of constituent atoms of a spin moment S. We take here $S = \mu_{\mathrm{Co}} \simeq 1.7\mu_{\mathrm{B}}$. We can bind then N, N_{SP}, and the PM Co concentration by the requirement that the total density of the

Co atoms in the volume of the layer, $N_0 x_{\rm eff}(300\ {\rm K}) + N N_{\rm SP}$, is equal to the Co concentration found by SIMS in this layer, $x^{\rm SIMS}({\rm FM\text{-}2}) = 8\%$. Therefore, out of three, N, $N_{\rm SP}$, and $x_{\rm eff}(300\ {\rm K})$, we are left with two temperature and field-independent adjustable parameters, which are established by numerical fitting to the data for $H > 5$ kOe, as we do not have enough knowledge on the processes which determine coercivity and remanence at the blocked state of the SP ($T \lesssim 15$ K), hence on the magnitude of M at weak magnetic fields.

As detailed later in Fig. 16, the magnitude of the anisotropic interface contribution has been derived from the room temperature $M(H)$ of the thinnest of the layers grown at 200 °C (layer FM-3), for which the magnetic signal from the Co-enriched interface constitutes almost the entire magnetic response. This M is scaled accordingly to the both samples' *areas* and is subtracted from the data. Therefore, there are no fitting parameters here.

This relatively simple procedure provides a very good description at the whole temperature range, strongly indicating the correctness of the approach and that all three components to M are to the first order independent one from another. The best fit has been obtained with 35% of Co present in the bulk of the layer precipitating into the SP nanocrystals, whereas the remaining 65% assuming ZnO lattice cation sites. We also get $N \simeq 760$ Co atoms ($\mu \simeq 1300\mu_{\rm B}$) what gives the diameter of the nanocrystals, $d \simeq 2.5$ nm. Here, as well as in the further numerical assessments, we adopt material constants of bulk cobalt. In particular we share the view of Ney and co-workers[81] that Co crystals which are of 2- to 5-nm size should not show any pronounced reduction of the magnetization between helium and room temperature.

2. *Superparamagnetism*

The TM-rich nanocrystals are frequently found in (Zn,TM)O independently of the preparation method.[26,28,81–84] We take now, that the nanocrystals in the layers studied here are built of pure metallic Co. For their size, neglecting the surface anisotropy,[85] there will be a single domain within each of them, and so they can be treated as rigid, temperature-independent dipole moments, the superspins of magnitude μ, randomly directed along a local, specific to each nanocrystal's crystalline or shape-dictated magnetic easy axis.

We have already indicated the presence of the superparamagnetic (SP) response during the modeling of the $M(H,T)$ data for sample FM-2 (Fig. 14). To substantiate this claim we turn now to another layer grown at 200 °C, which does not show any noticeable contribution from the low field and high-temperature anisotropic FM-like signal. The relevant findings are presented in Fig. 15, where the single-particle blocking is evidenced by a clear and quite sharp maximum of ZFCM at about $T_{\rm m} \simeq 8$ K and a featureless steady decrease of FCM on T around $T_{\rm m}$, much in a PM-like fashion. Employing the widely accepted formulas for DC-type SQUID magnetometry, $T_{\rm B} \simeq T_{\rm m} \simeq K V_{\rm nc}/25k_{\rm B}$, we obtain the average size of Co nanocrystals of 2.3 nm. It corresponds favorably to our previous estimate of 2.5 nm, obtained from Co atoms counting performed for a different layer, confirming the validity of our approach and indicating a universal constitution of our layers.

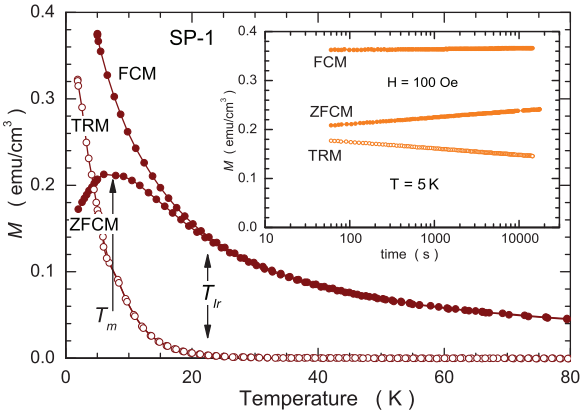

FIG. 15. (Color online) Blocking phenomenon in a superparamagnetic sample (SP-1). (Main part) Temperature dependence of the zero field cooled (ZFCM), field cooled (FCM), and thermoremnant (TRM) magnetization. For a monodispersed ensemble $T_{\rm m}$ corresponds to mean blocking temperature. Here, $T_{\rm Ir}$ corresponds to the maximum volume of statistically relevant nanogranules. (Inset) Time evolution of the magnetization in these three magnetic states measured at 5 K (below $T_{\rm m}$).

A much more rigorous confirmation that this is indeed the single-particle dynamical slowing down requires a laborious investigations in time domain,[86] which might rather go in vain here due to, primarily, not narrow enough size distribution of the nanocrystals and not truly single phase nature of the layers. We can, however, advocate for the SP origin of the magnetic signal in question by presenting a qualitative picture of time dependence of ZFCM, FCM, and TRM below $T_{\rm m}$, presented in the inset to Fig. 15. The reported there lack of noticeable relaxation of the FCM and relatively fast relaxations

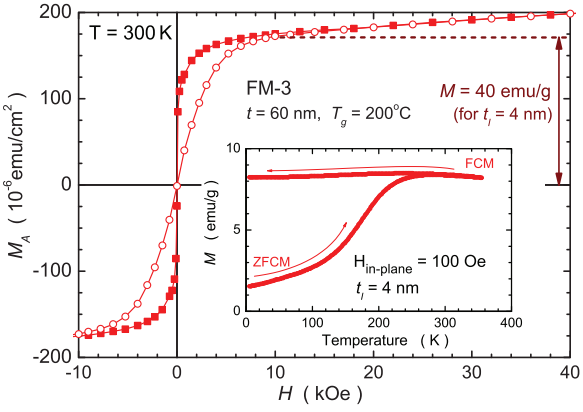

FIG. 16. (Color online) Magnetization of layer FM-3. (Main part) $M_{\rm A}$, the magnetic moment per unit area at 300 K. Solid squares are obtained with the magnetic field applied in the sample plane; open circles, in perpendicular configuration. The dashed horizontal line indicates the estimated saturation level of the near-the-interface part of the layer which we use in conjunction with the low field data ($|H| < 10$ kOe) to construct the standard data sets for this magnetic contribution $M_I(H)$, which has been employed in the modeling of the $M(H,T)$ presented in Fig. 14. The inset presents the low field in-plane zero field cooled (ZFCM) and field cooled (FCM) magnetization. The volume magnetization was obtained assuming the thickness of the Co-rich interface zone $t_I = 4$ nm.

of both ZFCM and TRM, upwards towards the FCM and downwards towards zero, respectively, indeed agree with the general expectations for the time evolution of these three types of magnetization in the blocked SP state.

3. *Interfacial ferromagnetism*

Figure 16 presents the room temperature $M(H)$ of the layer FM-3, the most suitable subject for examining the interface related magnetization since it is the thinnest one ($t \simeq 60$ nm) of all the layers hosting Co nanocrystals at the layer/substarte interface, so the corresponding magnetic response is the most prominent there. The anticipated planar origin of this signal is the reason we plot in Fig. 16 a "sheet" magnetization M_A, the magnetic moment per unit area, instead of the volume one. The advantage of this approach, as well as a further proof of the planar character of M_A, comes from a notion that we can eradicate this contribution from other layers by a simple subtraction of that established in Fig. 16 standard interface magnetization $M_I(H)$, providing it is scaled according to the layers' areas first. This magnetization exhibits a strong in-plane magnetic anisotropy, saturates swiftly below 10 kOe, is fairly temperature independent below 390 K (not shown here), and, within experimental resolution, exhibits virtually no coercivity ($H_C < 0.5$ Oe) or remanence [$M_A(0) < 10^{-3}$ of its saturation value]. As the $M(H)$, also the temperature dependence of M (see the inset to Fig. 16) differs considerably from M exhibited by the Co nanocrystals dispersed in the volume of the layer (cf. Fig. 15). Clearly, the $M(H)$ discussed here does resemble the signal from a thin, uniform layer of a soft high-T_C FM material. We additionally confirm here that quantitatively the same results are obtained for a sapphire-based sample.

However, despite such strong similarities, this magnetization does not originate from a continuous, metallic Co(-rich) film. Neither our characterization nor the available literature data for DMO[26,81–84] indicates a presence of such objects anywhere in the samples. On the contrary, *individual* Co nanocrystals decorating the interface are evidenced there. The lack of the continuous metallic layer here is finally confirmed by electrical measurements which indicate that none of our layers exhibits a metallic type of electrical conductivity (the FM-3 shows even no electrical conductivity at all; see Table I), so these nanocrystals do not physically percolate; they stay separated one from another. Finally, we note that a large disagreement observed between dc and ac microvave conductivity of these layers confirms the assessments about a discontinuous character of the interfacial Co layer (for details see Supplemental Material).[87–94]

So, why is the magnetic response of the standing alone interfacial Co nanocrystals so different from the superparamagnetism exhibited by the volume dispersed ones? We note, following Coey *et al.*,[20] that this question is generic for the whole class of high-T_C DMSs and DMOs. It has been argued by these authors that dipole interactions between macrospins occupying a small portion of the film volume may explain temperature-independent, coercive-less, and fast saturating $M(H)$. Our system fulfills these conditions: interfacial nanocrystals comparing to the volume ones exhibit a greater packing (volume) density ϵ (or, equivalently, in much smaller internanocrystal distance r), greater magnitude of the superspin moments (bigger volumes) but most notably in their two-dimensional (2D) arrangement on the interface. The first two factors dramatically enlarge the strength of the intersuperspin dipole-dipole interaction, making it comparable to the relevant energy scales in the system (thermal, anisotropy,. . . , etc).

For the two superspins their dipolar energy amounts to

$$E_{\mathrm{dd}} \simeq \mu^2/r^3 \cong \mu M \epsilon, \tag{4}$$

where M is the magnetization of a nanocrystal with the superspin moment $\mu = MV_{\mathrm{nc}}$. In order to evaluate the strength of the dipolar interaction for the interface nanocrystals we assess their volume fraction ϵ_I from the saturation level of the interface magnetization M_I (marked in Fig. 16 by a dashed line at $M_A^{\mathrm{sat}} \cong 160$ emu/cm^2), which we recalculate to the volume magnetization by taking for the thickness of the interfacial zone $t_I = d \simeq 4$ nm, the evidenced by HRTEM average diameter of the interfacial Co nanocrystals. The obtained value of $M_I^{\mathrm{sat}} = 40$ emu/g is a quarter of the bulk Co saturation magnetization, therefore with a good accuracy $\epsilon_I \simeq 0.25$ giving $E_{\mathrm{dd}}/k_{\mathrm{B}} \simeq 120$ K.

Such a large value of the dipolar energy E_{dd} means that the effects of the dipolar interaction are important even at elevated temperatures. In fact for such a dense 2D random dispersion of superspins a high-temperature dipolar in-plane ferromagnetic ordering has been predicted.[22] This dipolar superferromagnetism (DSFM) is even more likely to occur since the easy axes of the nanocrystals need not necessarily freeze in a truly random pattern. Instead, as they are set during the buildup of the layer they get correlated with the dipolar interactions which are already there. In other words, the final pattern contains an imprint of the dipolar forces and so additionally favors their ferromagnetic arrangement, most likely in a domainlike fashion,[95,96] accounting for vanishing coercivity and remanence, and so leading to fast saturation due to a swift domain rotations and domain walls annihilation in an external field. Interestingly, a qualitatively similar explanation was already put forward by Straumal and co-workers who also assigned the FM features of DMO to 2D-like structure(s) within the material: first to the grain boundaries in general,[97] but narrowed their view later to specific textures only.[98]

Indeed, ZnO when alloyed with TM assumes a highly grained structure, so there are plenty of grain boundaries within. However, the whole set presented in this paper experiment decisively contradicts this view. First, *all* our layers exhibit a similarly highly grained structure but those grown at lower T_g (as well as those of Risbud *et al.*[99]) exhibit no FM-like response whatsoever. More importantly, the FM-like features are absent independently whether the low-temperature grown layer has a strong texture or none at all. Clearly, all the FM characteristics presented here must have a more universal origin; they cannot be connected with details of the texture of the layer.

It is worth noting that similar planar dispersions of TM-rich nanocrystals were recently synthesized in the volume of GaN:Fe layers.[100,101]

This FM ordering accounts simultaneously for the strong in-plane magnetic anisotropy exhibited by the interfacial zone of the layer. Indeed, the experimentally observed anisotropy field, $H_{\mathrm{A}}^{\mathrm{exp}} \simeq 5$ kOe, is about 3.5 times—nearly the same factor

as for the volume reduction $1/\epsilon_I \simeq 4$—weaker than that of a solid Co film, $H_A^{\mathrm{Co}} \simeq 18.5$ kOe.

We have already highlighted the fact that the magnetic signal of the interfacial zone in our layers, $M_I(H)$, has a similar magnitude in all the samples we find, that is, independently of the growth time, and so of the thickness of the layer or absolute number of Co atoms provided during the growth. A similar finding has been reported in an extended study by Venkatesan and co-workers who found a fairly x_{TM}-independent surface component to the total magnetization in eight layers of $Zn_{1-x}Co_xO$ with x_{Co} ranging from 0.01 to 0.23.[102] Its magnitude differs only by 20% from the interface magnetization established in this study. In exactly the same 20%-wide band stay results inferred from the data of Lardé *et al.*[26] and Fukuma *et al.*[83] Generally, this observation elucidates the frequently reported property of DMO layers that the magnitude of the FM-like signal found there does not scale with the TM concentration when expressed per volume of the layer, or, in particular, the average moment per TM atom calculated in this way strongly decreases with increasing TM concentration in the sample; see Ref. 84 for an example of such behavior.

We finally observe here that the appearance of perfect ferromagnetic correlations without physical percolation among nanocrystals can be largely advantageous as it has a strong technological relevance. High permeability and low eddy current loss materials are in demand for various microelectronic devices desired for high frequencies and spintronics,[103] but there is a technological challenge to meet both requirements simultaneously.[104] In practice, extremely high packing densities are required to induce sizable internanocrystal exchange interactions, the key requirement to induce the long-range FM order in 3D systems without destroying the *nonpercolating* character of the dispersion.[105] Here, the 2D character of the dipolar correlation in a modestly dense ensemble of Co nanocrystals essentially does the same job, which points out that the ALD technique employed here allows for a cheap and semiconductor-industry-compatible method of mass production of such a technologically viable material.

VIII. CONCLUSIONS

In this work detailed studies of the magnetism origin have been reported for polycrystalline (Zn,Co)O grown by atomic layer deposition. It has been demonstrated that this method allows one, by changing the growth temperature, to obtain samples with rather different magnetic properties. Various ion-beam, synchrotron, electron microscopy, and spectroscopy tools have been exploited to find out mechanisms underlying magnetic behaviors.

The main conclusions of our work can be ordered as follows:

(1) The employed nanocharacterization methods have allowed one to demonstrate the presence of densely packed Co nanocrystals at the interface to the substrate in samples grown at 200 °C or higher temperatures. In these samples, ferromagneticlike features persisting to the above room temperature have been detected. By combining nanocharacterization data on interfacial Co nanocrystals with the model of *two-dimensional* dipolar superferromagnets it has been possible to explain pertinent characteristics of ferromagneticlike features: the high-temperature scale, the magnitude of saturation magnetization, the character of magnetic anisotropy, and the shape of hysteresis loops. It has been shown that this model also explains results obtained by other groups on (Zn,Co)O samples obtained by other growth methods.

(2) No interfacial Co nanocrystals have been detected in samples grown at 160 °C. Rather than showing ferromagnetic or superparamagnetic signatures, magnetic properties of such samples point to a random distribution of Zn-substitutional Co ions coupled by a strong but short-range antiferromagnetic interaction. By extending the previously studied range of Co concentrations up to $x = 0.4$, spin-glass freezing has been observed. In agreement with earlier studies, high Néel temperature is predicted for wz-CoO, $T_{\mathrm{N}} \approx 700$ K.

(3) No ferromagnetism that could be assigned to point or extended defects (e.g., grain boundaries) has been detected in the studied samples. However, a specific orientation of single crystalline grains affects substantially the paramagnetic anisotropy that can be accounted for by incorporating into theory information obtained from x-ray diffraction.

(4) Magnetic properties of a series of $(ZnO)_m(CoO)_n$ digital alloys ($m = 2,8, n = 1$) and superlattices ($m = 80, n = 5,10$) have been compared. The data provide evidence that the Co interdiffusion in the digital alloy structures is sufficient to produce truly random $Zn_{1-x}Co_xO$ mixed crystals with x up to 40%. In contrast, in the superlattice structures the interdiffusion is not strong enough to homogenize the Co content along the growth direction, which results in the formation of (Zn,Co)O films with spatially modulated Co concentrations.

In general terms, our results presented here as well as in parallel work on TM-doped nitrides,[7,21] reemphasize the necessity of using a range of nanocharacterization tools in order to assess the lateral *and* vertical distributions of TM ions in the studied films. A nonrandom distribution of TM atoms and a nonrandom distribution of TM-rich nanocrystals themselves underline relevant features of these systems, particularly their magnetic properties. These distributions depend sensitively on growth parameters and co-doping, which make it possible to obtain a variety of different materials, ranging from DMSs with a random distribution of magnetic cations to nanocomposites with specific magnetic properties.

ACKNOWLEDGMENTS

The work was supported by the European Research Council through the FunDMS Advanced Grant (Grant No. 227690) within the "Ideas" 7th Framework Programme of the European Common and by the European Regional Fund through grants from the Innovative Economy Operational Programme 2007–2013 (Grants No. POIG.01.01.02-00-008/08 and No. POIG.02.01-00-14-032/08), InTechFun (Grant No. POIG.01.03.01-00-159/08), and SemiSpinNet (Grant No. PITNGA-2008-215368). We also acknowledge the support of the Polish National Science Centre under

Grant No. 2011/03/D/ST3/02654 and the Carl Trygger's Foundation for Science Research. EXAFS and XANES research received funding from the European Community's 7th Framework Programme under Grant No. 226716. I.A. Kowalik acknowledges support from the Baltic Science Link project coordinated by the Swedish Research Council, VR.

*mikes@ifpan.edu.pl
†guzel@ifpan.edu.pl

[1]K. Sato and H. Katayama-Yoshida, Jpn. J. Appl. Phys. **39**, L555 (2000).
[2]K. Ueda, H. Tabata, and T. Kawaii, Appl. Phys. Lett. **79**, 988 (2001).
[3]S. J. Pearton, C. R. Abernathy, M. E. Overberg, G. T. Thaler, D. P. Norton, N. Theodoropoulou, A. F. Hebard, Y. D. Park, F. Ren, J. Kim, and L. A. Boatner, J. Appl. Phys. **93**, 1 (2003).
[4]T. Dietl, Nat. Mater. **2**, 646 (2003).
[5]C. Liu, F. Yun, and H. Morkoç, J. Mater. Sci. - Mater. El. **16**, 555 (2005).
[6]J. M. D. Coey, Current Opinion Solid State Mater. Sci. **10**, 83 (2006).
[7]A. Bonanni and T. Dietl, Chem. Soc. Rev. **39**, 528 (2010).
[8]T. Dietl, A. Haury, and Y. M. d'Aubigne, Phys. Rev. B **55**, R3347 (1997).
[9]T. Dietl, Nat. Mater. **9**, 965 (2010).
[10]M. Sawicki, T. Devillers, S. Gałęski, C. Simserides, S. Dobkowska, B. Faina, A. Grois, A. Navarro-Quezada, K. N. Trohidou, J. A. Majewski, T. Dietl, and A. Bonanni, Phys. Rev. B **85**, 205204 (2012).
[11]S. Koleśnik and B. Dąbrowski, J. Appl. Phys. **96**, 5379 (2004).
[12]A. Wójcik, K. Kopałko, M. Godlewski, E. Guziewicz, R. Jakieła, R. Minikayev, and W. Paszkowicz, Appl. Phys. Lett. **89**, 051907 (2006).
[13]A. Wójcik, M. Godlewski, E. Guziewicz, K. Kopałlko, R. Jakieła, M. Kiecana, M. Sawicki, M. Guziewicz, M. Putkonen, L. Niinisto, Y. Dumont, and N. Keller, Appl. Phys. Lett. **90**, 082502 (2007).
[14]J. H. Kim, H. Kim, D. Kim, Y. E. Ihm, and W. K. Choo, J. Appl. Phys. **92**, 6066 (2002).
[15]A. Ney, T. Kammermeier, K. Ollefs, S. Ye, V. Ney, T. C. Kaspar, S. A. Chambers, F. Wilhelm, and A. Rogalev, Phys. Rev. B **81**, 054420 (2010).
[16]P. Sati, C. Deparis, C. Morhain, S. Schäfer, and A. Stepanov, Phys. Rev. Lett. **98**, 137204 (2007).
[17]A. Ney, K. Ollefs, S. Ye, T. Kammermeier, V. Ney, T. C. Kaspar, S. A. Chambers, F. Wilhelm, and A. Rogalev, Phys. Rev. Lett. **100**, 157201 (2008).
[18]A. Ney, V. Ney, F. Wilhelm, A. Rogalev, and K. Usadel, Phys. Rev. B **85**, 245202 (2012).
[19]M. Sawicki, W. Stefanowicz, and A. Ney, Semicon. Sci. Technol. **26**, 064006 (2011).
[20]J. M. D. Coey, P. Stamenov, R. D. Gunning, M. Venkatesan, and K. Paul, New J. Phys. **12**, 053025 (2010).
[21]A. Navarro-Quezada, N. Gonzalez Szwacki, W. Stefanowicz, T. Li, A. Grois, T. Devillers, M. Rovezzi, R. Jakieła, B. Faina, J. A. Majewski, M. Sawicki, T. Dietl, and A. Bonanni, Phys. Rev. B **84**, 155321 (2011).
[22]A. V. Panov, Appl. Phys. Lett. **100**, 052406 (2012), and references therein.
[23]A. Ney *et al.*, New J. Phys. **12**, 013020 (2010).
[24]M. Venkatesan, P. Stamenov, L. S. Dorneles, R. D. Gunning, B. Bernoux, and J. M. D. Coey, Appl. Phys. Lett. **90**, 242508 (2007).
[25]K. Rode, R. Mattana, A. Anane, V. Cros, E. Jacquet, J.-P. Contour, F. Petroff, A. Fert, M.-A. Arrio, P. Sainctavit, P. Bencok, F. Wilhelm, N. B. Brookes, and A. Rogalev, Appl. Phys. Lett. **92**, 012509 (2008).
[26]R. Lardé, E. Talbot, P. Pareige, H. Bieber, G. Schmerber, S. Colis, V. Pierron-Bohnes, and A. Dinia, J. Am. Chem. Soc. **133**, 1451 (2011).
[27]H. J. von Bardeleben, N. Jedrecy, and J. L. Cantin, Appl. Phys. Lett. **93**, 142505 (2008).
[28]S. Zhou, K. Potzger, J. von Borany, R. Grötzschel, W. Skorupa, M. Helm, and J. Fassbender, Phys. Rev. B **77**, 035209 (2008).
[29]M. Godlewski, E. Guziewicz, M. I. Łukasiewicz, I. A. Kowalik, M. Sawicki, B. S. Witkowski, R. Jakieła, W. Lisowski, J. W. Sobczak, and M. Krawczyk, Phys. Status Solidi B **248**, 1596 (2011).
[30]T. C. Kaspar, T. Droubay, S. M. Heald, M. H. Engelhard, P. Nachimuthu, and S. A. Chambers, Phys. Rev. B **77**, 201303 (2008).
[31]T. Dietl, T. Andrearczyk, A. Lipińska, M. Kiecana, M. Tay, and Y. Wu, Phys. Rev. B **76**, 155312 (2007).
[32]M. P. Proenca, C. T. Sousa, A. M. Pereira, P. B. Tavares, J. Ventura, M. Vazquez, and J. P. Araujo, Phys. Chem. Chem. Phys. **13**, 9561 (2011).
[33]L. Li, Y. Guo, X. Y. Cui, R. Zheng, K. Ohtani, C. Kong, A. V. Ceguerra, M. P. Moody, J. D. Ye, H. H. Tan, C. Jagadish, H. Liu, C. Stampfl, H. Ohno, S. P. Ringer, and F. Matsukura, Phys. Rev. B **85**, 174430 (2012).
[34]See Supplemental Material at http://link.aps.org/supplemental/10.1103/PhysRevB.88.085204 for additional information on the employed experimental procedures, the theoretical model, and additional experimental results of TEM, SQUID, and ac conductivity measurements.
[35]J. K. Furdyna, J. Appl. Phys. **64**, R29 (1988).
[36]A. Lewicki, A. I. Schindler, I. Miotkowski, and J. K. Furdyna, Phys. Rev. B **41**, 4653 (1990).
[37]T. Dietl, in *Handbook of Semiconductors*, edited by S. Mahajan, Vol. 3B (North Holland, Amsterdam, 1994), p. 1251.
[38]B. B. Straumal, A. A. Mazilkin, S. G. Protasova, P. B. Straumal, A. A. Myatiev, G. Schütz, E. J. Goering, T. Tietze, and B. Baretzky, Phil. Mag. **93**, 1371 (2013).
[39]M. I. Łukasiewicz, A. Wójcik-Głodowska, E. Guziewicz, A. Wolska, M. T. Klepka, P. Dłużewski, R. Jakieła, E. Łusakowska, K. Kopalko, W. Paszkowicz, Ł. Wachnicki, B. S. Witkowski, W. Lisowski, M. Krawczyk, J. W. Sobczak, A. Jabłoński, and M. Godlewski, Semicon. Sci. Technol. **27**, 074009 (2012).
[40]P. Scherrer, Göttinger Nachrichten Gesell. **2**, 98 (1918).
[41]I. Kowalik, E. Guziewicz, K. Kopałko, S. Yatsunenko, A. Wójcik-Głodowska, M. Godlewski, P. Dłużewski, E. Łusakowska, and W. Paszkowicz, J. Cryst. Growth **311**, 1096 (2009).

[42] A. Bonanni, M. Kiecana, C. Simbrunner, T. Li, M. Sawicki, M. Wegscheider, M. Quast, H. Przybylińska, A. Navarro-Quezada, R. Jakieła, A. Wołoś, W. Jantsch, and T. Dietl, Phys. Rev. B **75**, 125210 (2007).

[43] B. Ravel and M. Newville, J. Synchrotron Rad. **12**, 537 (2005).

[44] A. L. Ankudinov, B. Ravel, J. J. Rehr, and S. D. Conradson, Phys. Rev. B **58**, 7565 (1998).

[45] J. Rehr, J. Kas, F. Vila, M. Prange, and K. Jorissen, Phys. Chem. Chem. Phys. **12**, 5503 (2010).

[46] A. Wolska, M. T. Klepka, B. S. Witkowski, M. I. Łukasiewicz, E. Guziewicz, and M. Godlewski, Acta Phys. Pol. A **121**, 883 (2012).

[47] S. Hüfner, *Photoemission Spectroscopy* (Springer, Berlin, 2003).

[48] A. V. Naumkin, A. Kraut-Vass, S. W. Gaarenstroom, and C. J. Powell, NIST Standard Reference Database 20, Version 4.1, http://srdata.nist.gov/xps/ (2008).

[49] M. S. B. J. Tan and K. J. Klabunde, J. Am. Chem. Soc. **113**, 855 (1991).

[50] I. A. Kowalik, G. Öhrwall, B. N. Jensen, R. Sankari, E. Wallén, U. Johansson, O. Karis, and D. Arvanitis, J. Phys: Conf. Ser. **211**, 012030 (2010).

[51] M. Kobayashi, Y. Ishida, J. I. Hwang, Y. Osafune, A. Fujimori, Y. Takeda, T. Okane, Y. Saitoh, K. Kobayashi, H. Saeki, T. Kawai, and H. Tabata, Phys. Rev. B **81**, 075204 (2010).

[52] A. M. Mulders, H. Loosvelt, A. F. Rodrguez, E. Popova, T. Konishi, K. Temst, O. Karis, D. Arvanitis, and C. V. Haesendonck, J. Phys.: Condens. Matter **21**, 124211 (2009).

[53] M. Opel, K.-W. Nielsen, S. Bauer, S. Goennenwein, J. Cezar, D. Schmeisser, J. Simon, W. Mader, and R. Gross, Euro. Phys. J. B **63**, 437 (2008).

[54] T. Estle and M. De. Wit, Bull. Am. Phys. Soc. **6**, 445 (1961).

[55] J. Spałek, A. Lewicki, Z. Tarnawski, J. K. Furdyna, R. R. Gałązka, and Z. Obuszko, Phys. Rev. B **33**, 3407 (1986).

[56] R. N. Bhatt, Phys. Scr., T **14**, 7 (1986).

[57] J. R. Anderson, M. Górska, L. J. Azevedo, and E. L. Venturini, Phys. Rev. B **33**, 4706 (1986).

[58] P. Koidl, Phys. Rev. B **15**, 2493 (1977).

[59] S. W. Yoon, S.-B. Cho, S. C. We, S. Yoon, B. J. Suh, H. K. Song, and Y. J. Shin, J. Appl. Phys. **93**, 7879 (2003).

[60] A. Lewicki, A. I. Schindler, J. K. Furdyna, and W. Giriat, Phys. Rev. B **40**, 2379 (1989).

[61] J. A. Gaj, R. Planel, and G. Fishman, Solid State Commun. **29**, 435 (1979).

[62] T. Dietl, H. Ohno, F. Matsukura, J. Cibert, and D. Ferrand, Science **287**, 1019 (2000).

[63] P. Gopal and N. A. Spaldin, Phys. Rev. B **74**, 094418 (2006).

[64] D. Iuşan, M. Kabir, O. Grånäs, O. Eriksson, and B. Sanyal, Phys. Rev. B **79**, 125202 (2009).

[65] R. R. Gałązka, S. Nagata, and P. H. Keesom, Phys. Rev. B **22**, 3344 (1980).

[66] A. Mycielski, C. Rigaux, M. Menant, T. Dietl, and M. Otto, Solid State Commun. **50**, 257 (1984).

[67] A. Twardowski, H. J. M. Swagten, W. J. M. de Jonge, and M. Demianiuk, Phys. Rev. B **36**, 7013 (1987).

[68] J. Jaroszyński, J. Wróbel, G. Karczewski, T. Wojtowicz, and T. Dietl, Phys. Rev. Lett. **80**, 5635 (1998).

[69] T. Fukumura, Z. Jin, M. Kawasaki, T. Shono, T. Hasegawa, S. Koshihara, and H. Koinuma, Appl. Phys. Lett. **78**, 958 (2001).

[70] P. M. Shand, A. Lewicki, I. Miotkowski, B. C. Crooker, and J. K. Furdyna, Phys. Rev. B **44**, 6152 (1991).

[71] J. A. Mydosh, *Spin Glasses: An Experimental Introduction* (Taylor and Francis, London, 1993).

[72] G. Karczewski, M. Sawicki, V. Ivanov, C. Ruester, G. Grabecki, F. Matsukura, L. Molenkamp, and T. Dietl, J. Supercond. Nov. Magn. **16**, 55 (2003).

[73] A. Bonanni, M. Sawicki, T. Devillers, W. Stefanowicz, B. Faina, T. Li, T. E. Winkler, D. Sztenkiel, A. Navarro-Quezada, M. Rovezzi, R. Jakieła, A. Grois, M. Wegscheider, W. Jantsch, J. Suffczyński, F. D'Acapito, A. Meingast, G. Kothleitner, and T. Dietl, Phys. Rev. B **84**, 035206 (2011).

[74] C. Zener, Phys. Rev. **81**, 440 (1951).

[75] C. Zener, Phys. Rev. **82**, 403 (1951).

[76] P. W. Anderson and H. Hasegawa, Phys. Rev. **100**, 675 (1955).

[77] P. W. Anderson, Phys. Rev. **79**, 350 (1950).

[78] J. B. Goodenough, J. Phys. Chem. Solids **6**, 287 (1958).

[79] J. Kanamori, J. Phys. Chem. Solids **10**, 87 (1959).

[80] R. Rammal and J. Souletie, *Magnetism of Metals and Alloys* (North-Holland, Amsterdam, 1982).

[81] A. Ney, A. Kovcs, V. Ney, S. Ye, K. Ollefs, T. Kammermeier, F. Wilhelm, A. Rogalev, and R. E. Dunin-Borkowski, New J. Phys. **13**, 103001 (2011).

[82] S. R. Shinde, S. B. Ogale, J. S. Higgins, H. Zheng, A. J. Millis, V. N. Kulkarni, R. Ramesh, R. L. Greene, and T. Venkatesan, Phys. Rev. Lett. **92**, 166601 (2004).

[83] Y. Fukuma, H. Asada, J. Yamamoto, F. Odawara, and T. Koyanagi, Appl. Phys. Lett. **93**, 142510 (2008).

[84] H. Wei, T. Yao, Z. Pan, C. Mai, Z. Sun, Z. Wu, F. Hu, Y. Jiang, and W. Yan, J. Appl. Phys. **105**, 043903 (2009).

[85] M. Jamet, W. Wernsdorfer, C. Thirion, D. Mailly, V. Dupuis, P. Mélinon, and A. Pérez, Phys. Rev. Lett. **86**, 4676 (2001).

[86] T. Jonsson, P. Nordblad, and P. Svedlindh, Phys. Rev. B **57**, 497 (1998).

[87] K. S. Champlin and R. R. Krongard, IRE Trans. Microwave Theory Tech. **9**, 545 (1961).

[88] M. E. Brodwin and M. K. Parsons, J. Appl. Phys. **36**, 494 (1965).

[89] L. I. Buravov and I. F. Shchegolev, Instrum. Exp. Tech. **14**, 528 (1971).

[90] M. Jaworski and Z. Romaszewski, in *Organic Conductors and Semiconductors*, edited by L. Pal, G. Grüner, A. Janossy, and J. Solyom, Lecture Notes in Physics Vol. 65 (Springer, New York, 1977), p. 409.

[91] O. Kleiner, S. Donovan, M. Dressel, and G. Grüner, Intern. J. Infrared Millimeter Waves **14**, 2423 (1993).

[92] T. Gregorkiewicz and M. Jaworski, Radiat. Eff. **52**, 169 (1980).

[93] J. A. Osborn, Phys. Rev. **67**, 351 (1945).

[94] T. Gregorkiewicz, Ph.D thesis, Institute of Physics, PAS, Warsaw, 1979.

[95] M. A. Załuska-Kotur, Phys. Rev. B **54**, 1064 (1996).

[96] E. Bolcal, V. Dimitrov, B. Actaş, H. Aslan, and A. Bozkurt, Acta Phys. Pol. A **121**, 257 (2012).

[97] B. B. Straumal, A. A. Mazilkin, S. G. Protasova, A. A. Myatiev, P. B. Straumal, G. Schütz, P. A. van Aken, E. Goering, and B. Baretzky, Phys. Rev. B **79**, 205206 (2009).

[98] B. Straumal, A. Mazilkin, S. Protasova, A. Myatiev, P. Straumal, E. Goering, and B. Baretzky, Phys. Status Solidi B **248**, 1581 (2011).

[99] A. S. Risbud, N. A. Spaldin, Z. Q. Chen, S. Stemmer, and R. Seshadri, Phys. Rev. B **68**, 205202 (2003).

[100] A. Navarro-Quezada, W. Stefanowicz, T. Li, B. Faina, M. Rovezzi, R. T. Lechner, T. Devillers, F. d'Acapito, G. Bauer, M. Sawicki, T. Dietl, and A. Bonanni, Phys. Rev. B **81**, 205206 (2010).
[101] A. Navarro-Quezada, T. Devillers, T. Li, and A. Bonanni, Appl. Phys. Lett. **101**, 081911 (2012).
[102] M. Venkatesan, C. B. Fitzgerald, J. G. Lunney, and J. M. D. Coey, Phys. Rev. Lett. **93**, 177206 (2004).
[103] H. Fujimori, S. Ohnuma, N. Kobayashi, and T. Masumoto, J. Magn. Magn. Mater. **304**, 32 (2006).
[104] S. Bedanta, T. Eimüller, W. Kleemann, J. Rhensius, F. Stromberg, E. Amaladass, S. Cardoso, and P. P. Freitas, Phys. Rev. Lett. **98**, 176601 (2007).
[105] M. R. Scheinfein, K. E. Schmidt, K. R. Heim, and G. G. Hembree, Phys. Rev. Lett. **76**, 1541 (1996).